In Vivo Quantification of Cell Coupling in Plants with Different Phloem-Loading Strategies[W][OA]

Johannes Liesche and Alexander Schulz*

Department of Plant Biology and Biotechnology, University of Copenhagen, DK–1871 Frederiksberg C, Denmark

Uptake of photoassimilates into the leaf phloem is the key step in carbon partitioning and phloem transport. Symplasmic and apoplasmic loading strategies have been defined in different plant taxa based on the abundance of plasmodesmata between mesophyll and phloem. For apoplasmic loading to occur, an absence of plasmodesmata is a sufficient but not a necessary criterion, as passage of molecules through plasmodesmata might well be blocked or restricted. Here, we present a noninvasive, whole-plant approach to test symplasmic coupling and quantify the intercellular flux of small molecules using photoactivation microscopy. Quantification of coupling between all cells along the prephloem pathways of the apoplasmic loader *Vicia faba* and *Nicotiana tabacum* showed, to our knowledge for the first time in vivo, that small solutes like sucrose can diffuse through plasmodesmata up to the phloem sieve element companion cell complex (SECCC). As expected, the SECCC was found to be symplasmically isolated for small solutes. In contrast, the prephloem pathway of the symplasmic loader *Cucurbita maxima* was found to be well coupled with the SECCC. Phloem loading in gymnosperms is not well understood, due to a profoundly different leaf anatomy and a scarcity of molecular data compared with angiosperms. A cell-coupling analysis for *Pinus sylvestris* showed high symplasmic coupling along the entire prephloem pathway, comprising at least seven cell border interfaces between mesophyll and sieve elements. Cell coupling together with measurements of leaf sap osmolality indicate a passive symplasmic loading type. Similarities and differences of this loading type with that of angiosperm trees are discussed.

Phloem transport plays a crucial role in the coordination of plant growth and response to abiotic and biotic stressors by providing a continuous pathway to all organs for carbon distribution and signaling (Furch et al., 2007; Dinant and Lemoine, 2010; Ainsworth and Bush, 2011). For phloem function, the loading of the osmotically active transport sugars into the phloem is a key step (Ayre, 2011). It creates the hydrostatic pressure gradient between source and sink organs, which drives the mass flow of phloem sap, as already postulated by Münch (1930). For many herbaceous plants, it is well established that phloem transport is energized and regulated by an active loading step between bundle sheath cells (BSCs) and the sieve element companion cell complex (SECCC). Less is known about the prephloem pathway (i.e. the cell-to-cell transport of sugars from the mesophyll to the vascular bundles). A symplasmic pathway for prephloem transport is assumed (Ayre, 2011; Chen et al., 2012), but all cells on that pathway seem to be able to take up Suc from the apoplast, which would allow for apoplasmic steps or a mixed apoplasmic/symplasmic prephloem transport (Orlich et al., 1998).

Two strategies of phloem loading, apoplasmic and symplasmic, have been defined based on the abundance of cell connections between the BSC and SECCC (Schulz, 2005). In symplasmic loaders, many plasmodesmata are present at this interface; therefore, it is assumed that Suc, the primary product of photosynthesis, can reach the phloem by cell-to-cell diffusion (Turgeon and Hepler, 1989). In apoplasmic loaders, no or only a few plasmodesmata are present at the BSC-SECCC interface. Since Suc cannot reach the phloem symplasmically, it has to be actively taken up by Suc transporters (Giaquinta, 1979; Delrot and Bonnemain, 1981; van Bel, 1993; Dinant and Lemoine, 2010; Turgeon, 2010).

Even though the SECCC of herbaceous symplasmic loaders are well coupled to the BSC, they are able to accumulate sugars actively in the phloem. According to the so-called polymer-trap mechanism, Suc enters the intermediary cell-type companion cells (CCs) by diffusion and is then converted into higher M_r sugars, mainly raffinose and stachyose (Turgeon and Beebe, 1991; Turgeon et al., 1993; Turgeon and Wolf, 2009). Those sugars are too large to diffuse back into the bundle sheath but can pass on through the specialized plasmodesmata-pore contacts into the sieve elements (SEs) to be transported in the phloem.

Both strategies of active loading result in a two to five times higher sugar concentration in phloem compared with the surrounding mesophyll (Geiger et al., 1973; Gamalei, 1989; Haritatos et al., 1996; Voitsekhovskaja et al., 2006). Active loading and a concomitant low sugar concentration in the mesophyll match the

* Corresponding author; e-mail als@life.ku.dk.

The author responsible for distribution of materials integral to the findings presented in this article in accordance with the policy described in the Instructions for Authors (www.plantphysiol.org) is: Alexander Schulz (als@life.ku.dk).

[W] The online version of this article contains Web-only data.

[OA] Open Access articles can be viewed online without a subscription.

www.plantphysiol.org/cgi/doi/10.1104/pp.112.195115

 © 2012 American Society of Plant Biologists. All Rights Reserved.

rapid-growth strategy of herbaceous plants (Turgeon, 2010). Active symplasmic loading is indicated whenever a plant has sugar polymers as main transport sugars.

More recently, a different mode of symplasmic loading was identified, which does not rely on active loading to establish a source-sink differential but maintains a high Suc concentration in all cells of the leaf (Turgeon and Medville, 1998; Rennie and Turgeon, 2009). This passive symplasmic loading has been primarily associated with woody angiosperm species (Rennie and Turgeon, 2009; Fu et al., 2011).

Structural methods alone have proved to be insufficient to characterize phloem loading (Gamalei, 1989; Schulz et al., 1998; Schulz, 2005). While the absence of plasmodesmata is clear evidence for a domain border in any tissue, their presence does not necessarily indicate free exchange within an individual symplasmic domain, as permeability through plasmodesmata can be dynamic (Schulz, 1999; Roberts and Oparka, 2003). Since it was shown that some apoplasmic loaders have abundant plasmodesmata between phloem and mesophyll (Rennie and Turgeon, 2009), plasmodesmal frequencies were proposed to be a feature of leaf anatomy rather than an indicator for the mode of phloem loading (Turgeon and Medville, 2004). Unrestricted flux through plasmodesmata in apoplasmic loaders would raise the question of how Suc transporters can maintain a high concentration in the phloem: any backflow of sugars would compromise loading efficiency.

The most reliable method to assess plasmodesmal functionality and regulation in a tissue uses radioactive sugars as tracers, but this is limited to homogenous tissues without competing phloem strands, as for example at the root tip, where the phloem stands end (Schulz, 1994, 1995).

Fluorescent tracers with size and diffusion properties similar to Suc, such as fluorescein and derivatives, have been used to assess symplasmic coupling since Schumacher's pioneering experiments on phloem transport in the 1930s (Schumacher, 1950), illustrating for instance the increasing control of plasmodesmal permeability in plant embryos and the development of domain borders in the shoot apex (Rinne and van der Schoot, 1998; Kim et al., 2005). Microinjection of tracer molecules into a target cell (Terry and Robards, 1987; Tucker et al., 1989; Goodwin et al., 1990; Ding et al., 1992; Duckett et al., 1994) and fluorescence recovery after photobleaching (FRAP) experiments with preloaded tracers (Pina et al., 2009; Rutschow et al., 2011) were used not only to test if neighboring cells are symplasmically connected but also to quantify coupling. Recently, three-dimensional photoactivation of the tracer fluorescein bis-(5-carboxymethoxy-2-nitrobenzyl) ether (caged fluorescein) was used to quantify plasmodesmata-mediated cell wall permeability between *Cucurbita maxima* leaf mesophyll cells (MCs; Liesche and Schulz, 2011). As this approach is less invasive than microinjection and is applicable to single cells in complex tissues, it was modified here to compare cell coupling in the prephloem pathway of different plant taxa.

Using this method, we were able to compare cell coupling all the way from the mesophyll along the prephloem pathway to the SECCC. Tracer flux along the prephloem pathway is indicative of the capacity for Suc diffusion up to the phloem (Ayre, 2011). Interfaces with low coupling were recognized as bottlenecks for transport and therefore as possible sites of regulation of carbon export.

In this paper, the strategies of phloem loading are validated by quantification of symplasmic coupling in the apoplasmic loaders *Vicia faba* and *Nicotiana tabacum* and the symplasmic loader *C. maxima*. Coupling in these herbaceous plants is then compared with that in the gymnosperm *Pinus sylvestris*, which has needle-formed leaves with xerophytic adaptations, like most gymnosperms. Neither the prephloem pathway nor the mode of phloem loading is characterized in gymnosperms yet (Liesche et al., 2011).

RESULTS

Photoactivation of single cells was performed to analyze cell coupling in plants with known phloem-loading modes, the apoplasmically loading *V. faba* and *N. tabacum* and the symplasmic loader *C. maxima*, and to identify the yet unknown loading type of *P. sylvestris*. After loading caged fluorescein into all leaf cells (Martens et al., 2004), leaves still attached to the plant, or detached from it, were transferred to the stage of a confocal microscope for imaging. Figure 1 shows a typical photoactivation experiment, consisting of three phases: (1) Preactivation: the field of view is illuminated with low-intensity excitation light (blue) to assess background fluorescence in the prospective emission range (green) of the activated tracer (Fig. 1A) and to acquire a bright-field image. The latter is used to focus and define the target cell to be photoactivated by drawing a region of interest (ROI; Fig. 1D). (2) Activation: the target cell is illuminated with a high-intensity UV laser for 25 to 60 s while continuing to record tracer signal in the field of view with low-intensity excitation light (Fig. 1B). (3) Postactivation: the whole field of view including the ROI is recorded with low-intensity excitation light for a further 25 to 60 s (Fig. 1C). This phase is also characterized by an accumulation of the tracer in chloroplasts of the observed cell. The development of fluorescence during photoactivation (Fig. 1E, gray area) is accompanied by its transfer via plasmodesmata into neighboring cells. Additional fluorescence in the target cell as caused by the strong UV illumination, which activates the tracer but also excites the activated tracer to a certain degree, is corrected for (Fig. 1E, stippled line). In the neighboring cells, fluorescence increases over time during activation of the target cell, despite some loss toward the second neighbors that is obvious after the end of photoactivation (Fig. 1F).

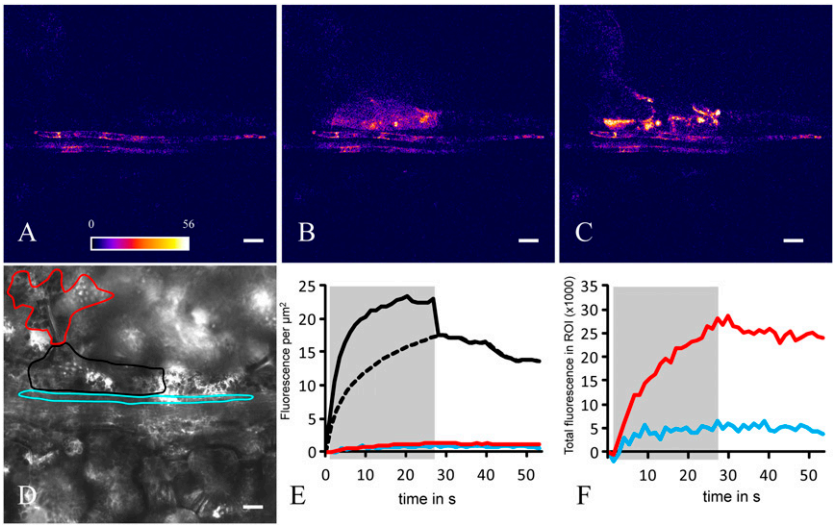

Figure 1. Photoactivation experiment to measure coupling between cells in the *N. tabacum* leaf. Before photoactivation (A), GFP fluorescence is present in CCs, which helps to identify this cell type. During photoactivation (B) in the bundle sheath target cell (see black outline in D) and after photoactivation (C), the fluorescence signal of the activated tracer spreads to neighboring cells. The ROIs corresponding to the target cell (black) and a directly neighboring CC (blue) and MC (red) are delineated on a bright-field image (D). The signal concentration and total fluorescence development in the respective cells over the course of the experiment are shown in E and F. The target cell signal is influenced by UV excitation during photoactivation (solid line on gray shading) and therefore replaced by a logarithmic increase (dashed line). From concentration potential and flux and interface length, a CCF is calculated. Bars = 20 μm.

Visualization of Cell Coupling in the Prephloem Pathway of Apoplasmic and Symplasmic Angiosperms

Intimate cell coupling can be appreciated when playing time series (*xyt*; the two spatial dimensions *x*, *y* over time *t*) of photoactivation experiments as time-lapse movies (Supplemental Movie S1). Figure 2 depicts images of target cells with their neighbors just at the start of postactivation. Cell types were primarily identified based on cell shape and relative location as seen on bright-field images (Fig. 2, A–C, G–I, and M–O). This is easy in case of MC, since they are bordering the intercellular space, and of BSC that have a characteristic shape (Fig. 2, first and second columns, respectively). The identification of CCs is more difficult. The transfer-type CCs in *V. faba* might be confused with phloem parenchyma cells, both being neighbors to SEs, but are identified by their tight association with the SEs (Fig. 2C; Supplemental Fig. S1). To discriminate CCs from phloem parenchyma cells in minor veins of *N. tabacum*, a plant line stably expressing GFP specifically in the endoplasmic reticulum of CCs was used (Figs. 1 and 2L). In the veins of *C. maxima*, intermediary-type CCs (Schulz, 2005) are larger than phloem parenchyma cells that are located above and below the image plane when SEs are in focus (Turgeon et al., 1993; Fig. 2O).

In all three plant species, coupling between MC and between MC and BSC was evident as flux of the tracer into the neighbor cells (Fig. 2, first and second column). In contrast to *C. maxima*, where fluorescein from the CC easily spread into the surrounding cells, and vice versa (Fig. 2R; Supplemental Fig. S2), only minor amounts of fluorescence were visible in the neighboring BSC in *V. faba* (Fig. 2F) and *N. tabacum* (Fig. 2L). In all plant species investigated, the tracer appeared instantaneously in the SE once it was visible/photoactivated in the CC (Supplemental Fig. S2; Supplemental Movie S1).

These observations indicate high coupling in the prephloem pathways of all three plant species up to the BSC-CC interface. While diffusion between SECCC and BSC of *V. faba* and *N. tabacum* was highly restricted, the symplasmic loader *C. maxima* showed an intimate coupling across this interface.

Visualization of Cell Coupling in the Prephloem Pathway of *P. sylvestris*

The prephloem pathway of needle-bearing gymnosperms is different from all angiosperm species, since it involves at least seven interfaces between mesophyll and SE and includes two particular cell types only occurring in gymnosperms, the transfusion parenchyma and Strasburger cells (Fig. 3A; Liesche et al., 2011). Moreover, there are no minor veins, but the vascular tissue is located inside a central stele. Bundle sheaths bordering the stele cells have characteristic Casparian strips, excluding the possibility that photoassimilates enter vascular tissue via the apoplast (Liesche et al., 2011). The transfusion parenchyma bridges the space between bundle sheath and the phloem, where Strasburger cells, flanking the SEs, mediate between transfusion parenchyma and SE. In single sections, the continuity of this symplasmic pathway

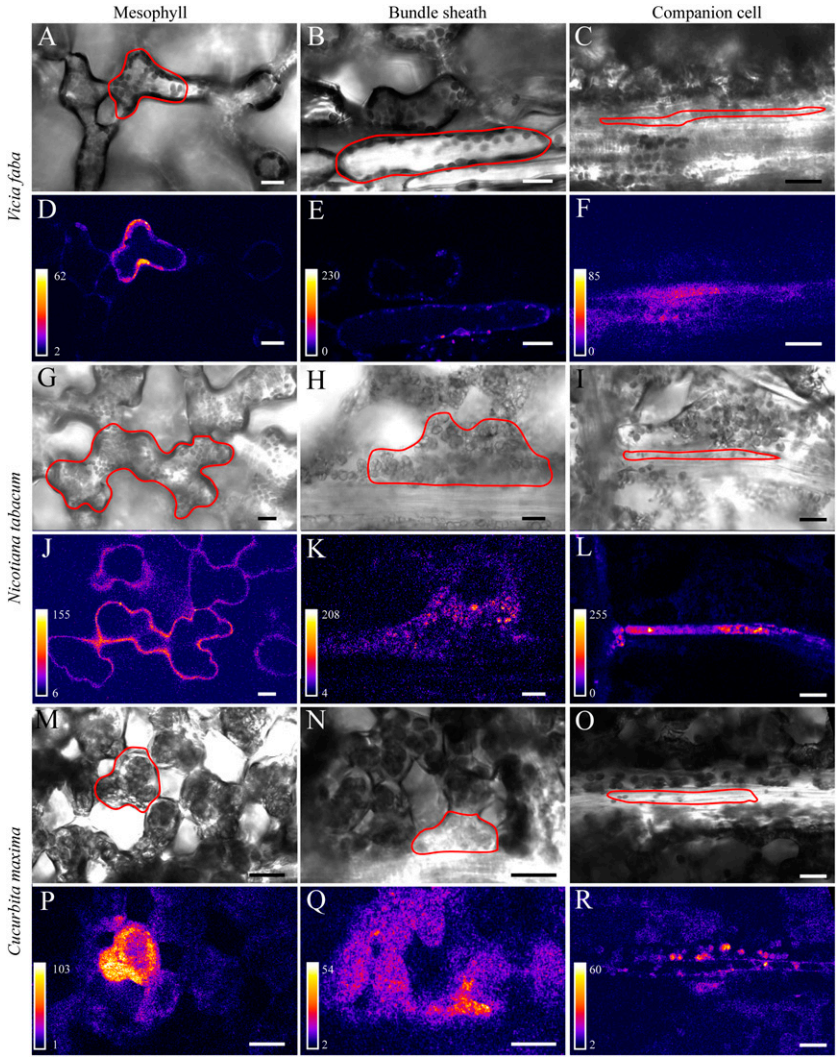

Figure 2. Postphotoactivation images from photoactivation experiments in *V. faba* (A–F), *N. tabacum* (G–L), and *C. maxima* (M–R). The respective target cells are outlined in the bright-field images (A–C, G–I, and M–O) that correspond to the fluorescence images shown directly below (D–F, J–L, and P–R). The first column of images shows photoactivation in MCs, the second column shows photoactivation in BSCs, and the third column shows photoactivation in CCs. In *N. tabacum*, GFP fluorescence is present in the CC in addition to tracer fluorescence (L), which can be subtracted and therefore does not influence the calculation of cell coupling. Note that only minor amounts of tracer signal are visible in neighboring BSCs after photoactivation in CCs in the apoplasmic loader *V. faba* (F) and *N. tabacum* (L), whereas more fluorescence is visible in the symplasmic loader *C. maxima* (R). Bars = 20 μm.

might not be evident, since dead transfusion tracheids are interspersed with the transfusion parenchyma (Fig. 3A). Strasburger cells are associated with SE and seem to play a similar role to CCs, but they are not ontogenetically related to SE. In the needle, there are three rows of Strasburger cells, of which only the inner one shares a wall interface with SE (Schulz, 1990; Liesche et al., 2011). Prephloem transport accordingly starts in a MC and proceeds via BSC, at least two transfusion parenchyma cells, and three Strasburger cells to eventually reach a SE.

Using the same experimental approach, we visualized prephloem transport in the *P. sylvestris* needle. Because of the thick epidermis, it was necessary to cut a window into the abaxial side of the needle. Areas of interest were then imaged through one or two intact cell layers, minimizing the effect of preparation on coupling. In all experiments involving the different cell types of the prephloem pathway, the flux of uncaged fluorescein across the target cell-neighbor cell interface was visible already by eye and occurred in all directions (Fig. 3, C and G–I). This indicates the continuity of symplasmic transport throughout the prephloem pathway.

Quantification of Cell Coupling

Comparison of the loading types in different plant species cannot be based on visual impressions or the measurement of fluorescence intensity in whole-cell ROIs, since the cell sizes as well as the cytosol-to-vacuole ratios of the different cell types along the pathway are highly variable. For quantification of cell coupling in homogenous tissue, which would give an idea of the capacity of plasmodesmata-mediated permeation through cell walls, several parameters need to be known that are valid for FRAP (Rutschow et al., 2011) as well as for photoactivation of a cytosol tracer. For short-term photoactivation, the key value is the difference in the concentration potential between the target cell and the next neighbor, which can be derived from the respective fluorescence intensity. Using confocal microscopy and two-dimensional photoactivation, the distribution of the cytosol in a random optical section has a large effect on the coupling values as compared with a complete three-dimensional stack, in particular if the cell shapes are irregular (Liesche and

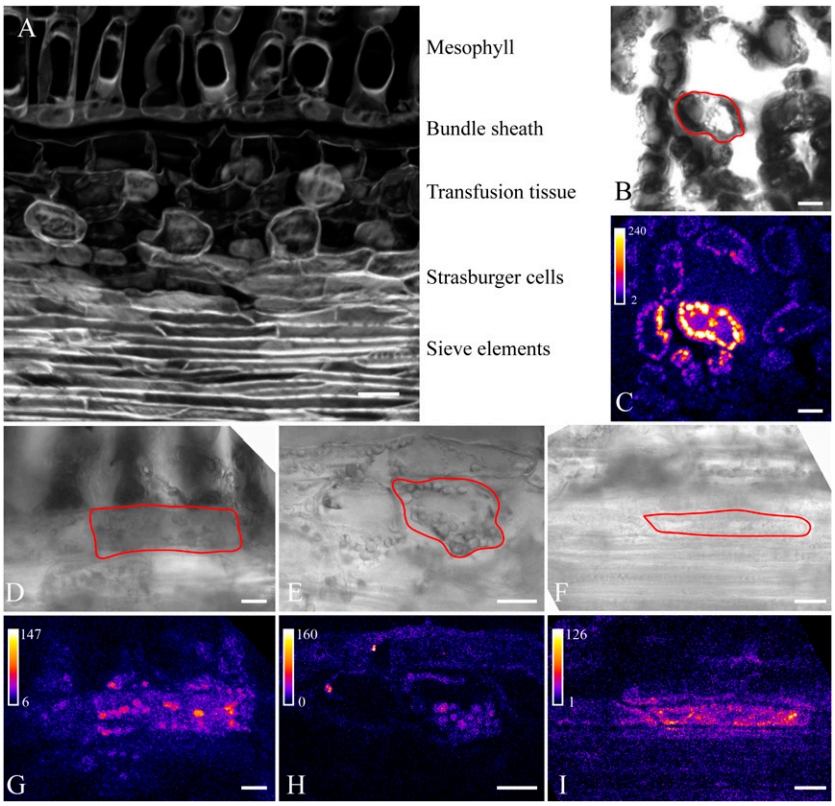

Figure 3. *P. sylvestris* needle anatomy in a longitudinal section (A) and postphotoactivation images of photoactivation experiments (B–I). The respective target cells are outlined in the bright-field images (B and D–F) that correspond to the fluorescence images shown directly below (C and G–I). Photoactivation in MCs (B and C), BSCs (D and G), transfusion parenchyma cells (E and H), and Strasburger cells (F and I) is shown. Note that fluorescence spreads to neighboring cells in all cases, including from Strasburger cells to SEs (I), indicating high symplasmic coupling along the prephloem pathway. Bars = 100 μm (A) and 20 μm (B–I).

Schulz, 2011). Long-term photoactivation in addition has to take into account the fact that the studied neighbor cell loses fluorescence to the next neighbors during the course of the experiment. In order to compensate for both problems, the quantification method presented by Liesche and Schulz (2011) for homogenous tissues was further developed. Loss to the neighbor cell is corrected by a cell type-specific correction factor, τ, derived from postphotoactivation fluorescence development. Differences in the cytosol-to-vacuole ratio, such as those between BSCs and CCs, are taken into account by correcting the fluorescence concentration values of target and neighbor cells. The fluorescence concentration $n = N\,V_c^{-1}$ relates the total cell fluorescence N to the cytosolic volume V_c, which was calculated with the help of experimentally determined, cell type-specific ratios of cell size to cytosolic volume. The cell coupling factor (CCF) is accordingly found in Equation 1:

$$\mathrm{CCF} = \frac{N_2^B \tau^B}{L_i} \frac{1}{(\bar{n}^A - \bar{n}^B)} \qquad (1)$$

with N_2^B indicating the total signal intensity in the neighbor cell in the first frame after photoactivation, L_i the interface length between the target cell (A) and the neighbor cell (B), τ^B correcting for the loss of tracer from the neighbor cell (B), and $\bar{n}^A$ and $\bar{n}^B$ giving the average fluorescence concentration in target and neighbor cells, respectively. This equation was derived from Fick's law of diffusion and simplified in that the interface area is replaced by the interface length and the length of plasmodesmata is neglected, since diffusion in the cytosolic compartment is the dominating factor for quantification at the cellular level (Rutschow et al., 2011). CCF has μm s^{-1} as a unit and is corrected for the different properties of the cells studied (see "Materials and Methods"). It cannot directly be compared with the plasmodesmata-mediated permeation value (Rutschow et al., 2011, Liesche and Schulz, 2011), which demands a complete three-dimensional analysis of the tracer distribution in target and neighbor cells and the interface area between them.

Table I compares the CCF measured along the prephloem pathways of the apoplasmic loaders *V. faba* and *N. tabacum*, the symplasmic loader *C. maxima*, and the as yet unidentified loader *P. sylvestris*. Only the coupling to the first neighbor cells of the target cell was analyzed, with a minimum of nine measurements per interface. The highest coupling was found between the small and cytosol-rich MCs of *C. maxima*, with a CCF of about 1 μm s^{-1}. While the MCs with one another and with the BSC were well coupled, with CCFs above 0.24 μm s^{-1}, a clear difference was seen at the interface between the BSC and SECCC of the angiosperms: here, the apoplasmic loaders had very small values (below 0.02 μm s^{-1}), while the symplasmic loader had a 10-fold higher CCF. This difference is highly significant, as tested by unpaired t test (Table I).

When comparing the two apoplasmic loaders *V. faba* and *N. tabacum*, the tracer flux in the former seemed to

Table I. *CCF of cell interfaces in the prephloem pathway*

Note the considerably smaller value between BSCs and CCs in *N. tabacum* and *V. faba*, indicating symplasmic isolation at this interface. Values are followed by SE and number of experiments in parentheses. M, Mesophyll; BS, bundle sheath; CC, companion cell; TP, transfusion parenchyma; Str, Strasburger cell; SE, sieve element. At the BS-CC interface, the difference between *V. faba* and *C. maxima* (*) and the difference between *N. tabacum* and *C. maxima* (**) are highly significant ($P = 0.0015$ and $P = 0.0025$, respectively). The difference between the two apoplasmic loaders is significant ($P = 0.015$; ***).

Cell Type	*V. faba*	*N. tabacum*	*C. maxima*	*P. sylvestris*
M-M	0.372 ± 0.035 (18)	0.492 ± 0.057 (22)	0.990 ± 0.219 (11)	0.591 ± 0.091 (21)
M-BS	0.239 ± 0.031 (14)	0.466 ± 0.061 (11)	0.955 ± 0.122 (18)	0.346 ± 0.038 (25)
BS-CC	0.007 ± 0.001 (9)*,***	0.017 ± 0.003 (14)**,***	0.194 ± 0.047 (15)*,**	
BS-BS				0.450 ± 0.068 (11)
BS-TP				0.463 ± 0.062 (17)
TP-TP				0.711 ± 0.092 (24)
TP-Str				0.606 ± 0.171 (14)
Str-Str				0.271 ± 0.046 (18)
Str-SE				0.302 ± 0.048 (10)

be nearly completely blocked while the latter showed some residual coupling. This difference was significant (Table I) and could be related to the closed minor-vein configuration of the former (i.e. transfer-type CC with virtually no plasmodesmata between SECCC and BSC), while the latter had an open minor-vein configuration with ordinary CC and some plasmodesmata (Gamalei, 1989; Schulz, 2005). The observed residual transport in *N. tabacum* could be an artifact, if the preparation conditions led to a pressure release from the phloem and, thus, relaxation of a pressure valve mechanism in the plasmodesmata between BSC and CC in *N. tabacum* (Oparka and Prior, 1992). This question could not be solved. In leaf cutouts, residual transport was larger than in leaves that still were attached to the plant. However, experiments stimulating or reducing callose production at sieve plates with Ca^{2+} or EGTA, respectively, did not significantly change the residual coupling values (data not shown).

In the gymnosperm, quantification of the coupling along the prephloem pathway showed that this pathway was well coupled up to the phloem, with values above 0.35 $\mu m\ s^{-1}$. There is no indication of symplasmic isolation, as seen at the BSC-CC interface of *V. faba* and *N. tabacum*, at any point along the pathway. The CCF for the BSC-transfusion parenchyma interface is in the same range of mesophyll and mesophyll-BSC interfaces. If there is a bottleneck, it is inside the phloem between the Strasburger cells, although this value is still higher than the CCF between BSC and SECCC in the symplasmic loader *C. maxima*. The intimate contact inside the SECCC made it impossible to derive a CCF in angiosperms (Supplemental Fig. S2), in contrast to the situation in *P. sylvestris*, where Strasburger cells and SEs only partially share cell wall interfaces (Table I).

Leaf Sap Osmolality in Gymnosperm Leaves

To further investigate the phloem-loading strategy of gymnosperms, leaf sap osmolality from two gymnosperm species were determined and compared with that in angiosperms. Active loaders generally have a lower leaf sap osmolality than passive loaders (Fu et al., 2011). In addition to needles from *P. sylvestris*, leaves of the tropical, broad-leafed gymnosperm tree *Gnetum gnemon* were included. There was a clear difference between the gymnosperm and angiosperm species tested (Fig. 4). Leaf sap osmolality of *P. sylvestris* and *G. gnemon* were more than twice as high as the actively loading *N. tabacum* and *V. faba*. Compared with average values for angiosperms with different phloem-loading types (Fu et al., 2011), *N. tabacum* and *V. faba* were below the average for active apoplasmic loaders, whereas *P. sylvestris* and *G. gnemon* were higher than the average Suc-transporting passive symplasmic loading trees (Fig. 4).

DISCUSSION

Quantification of Cell Coupling in Leaves with Photoactivation Microscopy

The benefit of measuring plasmodesmal permeability in a certain cell wall interface with fluorescent

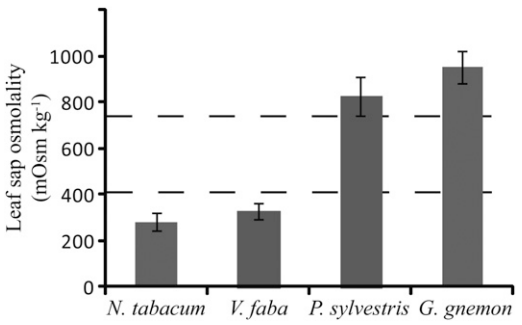

Figure 4. Leaf sap osmolality, measured at midafternoon, is significantly lower in the apoplasmic loading angiosperms *N. tabacum* and *V. faba* than in the gymnosperms *P. sylvestris* and *G. gnemon*. Average values for apoplasmic loaders and symplasmic loaders from Fu et al. (2011) are indicated by dashed lines. Error bars indicate SD.

tracers and FRAP, and the suitability of the calculation method used, were convincingly demonstrated by Rutschow et al. (2011): plasmodesmal transport is down-regulated after Trp and hydrogen peroxide treatment and in mutants known to have impaired plasmodesmal function. We used photoactivation microscopy to investigate cytosolic coupling between the different cell types in leaves from different plant species. The technique is noninvasive and has the advantage of providing a high dynamic range, making it especially suited to single-cell experiments in complex tissues. From tracer flux, diffusion potential, and anatomical parameters, a CCF was calculated, which characterizes the connectivity across a given cell wall interface.

The resulting values are not comparable to absolute values of plasmodesmata-mediated cell wall permeability, as derived from FRAP or photoactivation experiments for homogenous tissues. These are dependent upon knowledge of the interface area between the connected cells (Rutschow et al., 2011) and can be verified with three-dimensional recordings (three spatial dimensions x, y, and z over time t; Liesche and Schulz, 2011). In contrast to homogenous tissues such as the root cortex and leaf mesophyll, the prephloem pathway crosses compound tissues and passes cells that are different in size, shape, specialization, and interface areas. Challenges for developing a realistic coupling factor from single-plane movie recordings (xyt) were the unequal distribution of cytosol, potential tracer uptake into the vacuole, and diffusion into next-neighbor cells. The last two factors are compensated for by integrating a cell type-specific correction factor in the CCF calculation, which is based on postactivation changes of fluorescence intensity. Another potential error might be caused by the retention of tracer in target cell chloroplasts, but this influence is limited (Liesche and Schulz, 2011). With the CCF value, tracer flux is related to the shared cell wall length between neighboring cells. It might be argued that the CCF values are not comparable if the different interface areas vary strongly. However, it is assumed that equivalent cell borders, such as the BSC-CC interface border, have a comparable architecture, making CCF values across equivalent interfaces comparable between different plant species (for a discussion about the frequency of plasmodesmata/μm cell wall interface or plasmodesmata/μm vein, see Botha and van Bel, 1992).

The accuracy of all two-dimensional approaches is limited by out-of-focus photoactivation or out-of-focus bleaching in FRAP experiments. In conventional confocal microscopes, the excitation laser beam is focused on a point in the focus plane. Above and below, the beam widens in a cone shape, with photon density decreasing with distance from the focal plane (Pawley, 2006). Therefore, photoactivation can occur above and below the focal plane, and diffusion of the activated fluorescein into the imaging plane can influence the measurement (for a detailed discussion, see Testa et al., 2008). In the experiments presented here, it is unlikely that this effect had a significant impact (see below).

Cell Coupling along the Prephloem Pathway of Selected Angiosperm and Gymnosperm Species

In order to determine whether the prephloem pathway is open for symplasmic diffusion, we measured cell coupling between all cell types of that pathway in *V. faba*, *N. tabacum*, *C. maxima*, and *P. sylvestris* leaves. In schematic drawings, Figure 5 shows the outlines of the participating cells in longitudinal section and cross-section for each of the four plant species. The degree of cell coupling is indicated in the respective interfaces in heat map colors, spanning red (isolated) to yellow (intermediate) to green (well coupled), with 0.5 μm s^{-1} (coupling factor between MCs in *N. tabacum*) set as a reference for good coupling. Symplasmic coupling of all interfaces in the prephloem pathway of plants representing different loading types was quantified, to our knowledge, for the first time.

Recently, the identification of a Suc efflux carrier in Arabidopsis (*Arabidopsis thaliana*) provided new evidence on which route Suc takes from the site of synthesis in the MCs to the phloem CCs (Chen et al., 2012). The localization in phloem parenchyma cells indicates that only at this interface are sugars released into the apoplast, whereas the rest of the prephloem pathway can be assumed to be symplasmic (Braun, 2012). This notion is strongly supported by our results. In *N. tabacum* and *V. faba*, which are apoplasmic phloem loaders like Arabidopsis, high coupling should

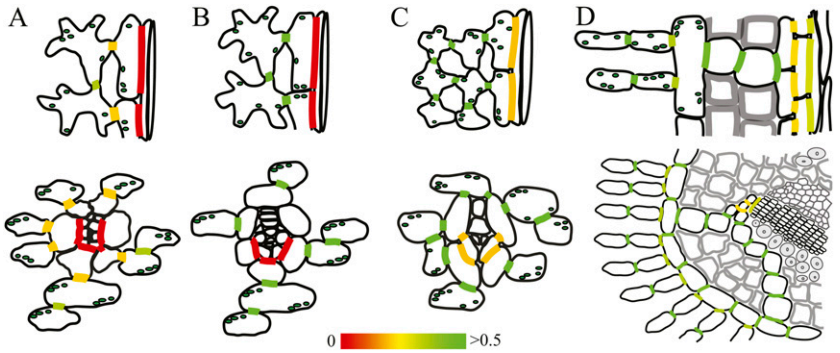

Figure 5. Cell coupling in the prephloem pathway. The color-coded coupling factors from Table I are shown on schematic drawings of collection phloem in longitudinal (top) and cross-sectional (bottom) views. Whereas the phloem of *V. faba* (A) and *N. tabacum* (B) is symplasmically isolated, all cells along the prephloem pathway are well coupled in *C. maxima* (C) and *P. sylvestris* (D).

ensure unrestricted Suc diffusion up to the SECCC cell wall (Fig. 5). There, the effective symplasmic isolation makes an apoplasmic step essential. Residual coupling at this interface in *N. tabacum* suggests that the plasmodesmata, present at this interface (Gamalei, 1989), do not contribute significantly to intercellular transport between CC and BSC. Plasmodesmata connecting the SECCC with the surrounding BSC would offer a futile backflow of Suc were passage through them unrestricted. It can only be speculated whether the residual transport seen here (1) indicates that plasmodesmata allow the escape of signal molecules from the SECCC toward the mesophyll or (2) just is a preparation artifact relaxing a pressure-valve mechanism in plasmodesmata (Oparka and Turgeon, 1999). The negligible transport across this interface in *V. faba*, which has a closed minor-vein configuration, is significantly lower than the residual transport in *N. tabacum* (Table I), confirming that photoactivation is indeed a reliable method to study cell coupling. The very small CCF value measured in *V. faba* (0.007 ± 0.001 $\mu m\ s^{-1}$) might be due to scattering of the UV laser light spot at cell walls or to out-of-focus photoactivation, but it shows that both factors are far too small to bias the coupling results.

As expected, there was no indication of an apoplasmic step anywhere in the *C. maxima* prephloem pathway. Nevertheless, the BSC-CC coupling was found to be markedly lower than between the other cells (Fig. 5), which might be related to the function of these plasmodesmata in the polymer-trap mechanism.

Our method was developed to assess the prephloem transport pathway and phloem-loading mode of *P. sylvestris* as a representative of gymnosperms and can be used for all plant species whose mode of phloem loading is not characterized yet. The whole prephloem pathway is well coupled and, accordingly, capable of accommodating a high flux rate for small solutes (Fig. 5). A polymer-trap mechanism can be excluded, as gymnosperms transport Suc and not sugar polymers as the main transport sugar (Shiroya et al., 1962; Schneider and Schmitz, 1989; Blechschmidt-Schneider et al., 1997; Willenbrink, 2002). Coupling values are smallest across the cell wall between Strasburger cells and between Strasburger cells and SE, indicating potential points of regulation. The unique structure of plasmodesmata at these interfaces supports such an assumption (Liesche et al., 2011).

Phloem Loading in *P. sylvestris*

Despite the economic and environmental importance of gymnosperms (Bhatnagar and Moitra, 1996; Jackson and Schlesinger, 2004), central aspects of their physiology are not characterized (Willenbrink, 2002). Regarding carbon partitioning, it is not known to what extent the anatomical differences, such as the xerophytic adaptation of their leaves, translate into physiological particularities of this group of plants. Instead of a branching minor vein system with up to seven vein classes and a concomitant high surface of the SECCC, needles have only one or two central vascular bundles, which are surrounded by a complex transfusion tissue and an endodermis-like bundle sheath (Fig. 3A; Liesche et al., 2011). In contrast to angiosperms, the SEs of gymnosperms do not have CCs but are associated to Strasburger cells, which flank the vascular bundles and are ontogenetically unrelated to the SE (Schulz, 1990; Liesche et al., 2011). Physiologically, the most important difference between angiosperm and gymnosperm leaves is the distance and number of cells between BSC and the phloem. In angiosperms, the SECCC of minor veins very often contacts the BSC directly or with only one intervening phloem parenchyma cell. In gymnosperms, two to three transfusion parenchyma and the same number of Strasburger cells have to be passed before assimilates approach the first SE. Moreover, the presence of Casparian strips in the BSC (Lederer, 1955; Wu et al., 2005; Liesche et al., 2011) excludes the possibility for sugars to reach the vascular tissue in the apoplast.

Combined with data on sugar level and distribution, a conclusive picture of phloem loading can be drawn. The high leaf sap osmolality found in *P. sylvestris* needles (Fig. 4) indicates a passive symplasmic loading mode. This cannot be due to a needle-typical, xerophytic adaptation, since *G. gnemon* has similar high values despite its broad leaves with a branching vein system (Liesche and Schulz, 2011). A high leaf sap osmolality was found in many angiosperm trees with this loading type (Fu et al., 2011). However, it cannot be excluded that woody plants, irrespective of their loading type, have a high leaf sap osmolality (Fu et al., 2011).

A decisive criterion for passive symplasmic loading is the Suc distribution in the leaf. According to the hypothesis, the concentration should be highest in the cytosol of MC to create a gradient that enables energetically downhill diffusion from MC into the SECCC (Rennie and Turgeon, 2009; Turgeon, 2010). The complex needle anatomy of *P. sylvestris* prevents a clean separation of all cell types, even with laser microdissection. Any measurement of Suc concentrations would need to discriminate between cytosol and vacuole, which can steepen and lower cytosolic Suc gradients. Suc transporters in the vacuolar membrane have been identified in poplar (*Populus* spp.) and other trees, which belong to the passive symplasmic loaders (according to Davidson et al. [2011]), and their significance for carbon export was demonstrated (Decourteix et al., 2006; Payyavula et al., 2011). In gymnosperms, Suc transporters have so far not been identified, but they are likely to be present (Shaukat et al., 1975; Canny, 1993).

It seems clear that *P. sylvestris*, a conifer model plant, employs a symplasmic loading type, and preliminary results suggest that the situation is similar in *G. gnemon* (J. Liesche, unpublished data). Since *Ginkgo biloba* also was suggested to load symplasmically by leaf-disc experiments (Blechschmidt-Schneider et al., 1997), it seems likely that all gymnosperms use this loading type.

Just as for angiosperm tree species, important questions regarding passive symplasmic loading in *P. sylvestris* remain to be solved. Is the sugar gradient between source and sink phloem just extended into the MCs in the leaf? How is phloem loading regulated? Answers to these questions can be expected from future experiments involving microautoradiography of needles fed with radioactively labeled CO_2, the identification and characterization of Suc transporters, and the expression of genetically encoded Suc sensors with binding affinities in the range of cytosolic concentrations (Okumoto, 2010).

MATERIALS AND METHODS

Photoactivation

Plant Growth

All plants were grown on soil under greenhouse conditions. *Vicia faba*, *Nicotiana tabacum* 'Samsun', and *Cucurbita maxima* were 4 to 8 weeks old. *Pinus sylvestris* seeds were vernalized for 2 months and then grown in 3 to 4 months to a height of at least 10 cm before they were used in the experiments. In order to identify CCs unambiguously, *N. tabacum* transformants expressing GFP under the control of the SUC2 promoter (Martens et al., 2006) were used in selected experiments.

Sample Preparation

Single leaves were glued upside down on a slide without detaching them from the plant using medical glue (Hollister). The leaf epidermis was partially removed, and 30 to 50 μL of fluorescein bis-(5-carboxymethoxy-2-nitrobenzyl) ether, dipotassium salt (CMNB-caged fluorescein; Invitrogen) was applied. In the case of *P. sylvestris* needles, an approximately 4-mm-long window was cut into the abaxial needle side by removing epidermis and mesophyll, but care was taken to preserve at least two intact cell layers above the observed area. Caged fluorescein was kept as a stock solution, with 1 mg dissolved in 100 μL of dimethyl sulfoxide, protected from light at −20°C. Right before use, 1 μL of stock solution was dissolved in 500 to 1,000 μL of phosphate-buffered saline, pH 7.2, for a final concentration of 10 to 20 μg mL^{-1}. A 20-min incubation under a coverslip and shielded from light was followed by several minutes of washing with phosphate-buffered saline, pH 7.2. The slide together with the whole plant was then placed on the microscope stage.

Imaging

A Leica SP2 or a Leica SP5X confocal laser-scanning microscope (Leica Microsystems) was used for all experiments. The UV lasers used for photoactivation (Coherent) were set to full power on the SP2 (40 mW at 351 and 364 nm) and to 70 mW at 355 nm on the SP5X. For imaging, the 488-nm line of the argon laser was used with 25% preset laser power and 15% gain of the acousto-optical tunable filter. Using the spectrometric filter, the detection window for fluorescence emission was set to 495 to 550 nm. A 40× dipping lens was used in all experiments, except for the high-resolution images (Supplemental Figs. S1 and S2), where a 63× water-immersion lens was used gain of the photomultiplier tube was set to somewhat below signal saturation, typically 700 to 800 V. For better image quality and stronger photoactivation effect, two times line averaging was activated. A time series consisting of prephotoactivation, photoactivation, and postphotoactivation phases was recorded, with photoactivation intervals varying between 35 and 60 s depending on cell type and plant species (Fig. 1).

Image Analysis

ROIs corresponding to the target cell and direct neighbors were defined using Volocity (Perkin-Elmer) and a Cintiq 21ux interactive pen display (Wacom; see Fig. 1D). The total fluorescence (integrated density) in each cell over the course of the photoactivation experiment was exported to Excel (Microsoft). The data were corrected for background fluorescence (autofluorescence and GFP signal in CCs of SUC2 transformants, respectively). In addition, the length of the interface between target and neighbor cells was measured.

The cytosolic area of cells in the image plane was determined with the help of the image-analysis software Volocity (Perkin-Elmer). An object detection algorithm (protocol "Find objects using intensity" with lower threshold at 10 and "Clip objects to ROI") was applied to the target cell on the first image after photoactivation, when all tracer-accessible areas in the cell show signal. This yields a value for the percentage of the total cell area that is accessible in a specific cell type (i.e. the cytosolic content of the cell).

Quantitative Analysis of Tracer Transport across Cell and Tissue Borders

The passive plasmodesmata-mediated permeation through cell walls is a straightforward diffusive process (Rutschow et al., 2011). Therefore, the rate of diffusion of small solute molecules like fluorescein or Suc across a barrier like the cell wall is given by Fick's law:

$$J = D\ A\ \frac{\Delta c}{\Delta x} \tag{2}$$

with the flux J in mol s^{-1}, the diffusion coefficient in the barrier D in μm^2 s^{-1}, the area of the barrier A in μm^2, the concentration potential of the diffusing substance Δc in mol μm^{-3}, and the diffusion distance Δx in μm.

The fluorescence signal intensity detected in a confocal microscope is directly proportional to the fluorochrome concentration (Pawley, 2006). Therefore, we here measure fluorescence flux Q and fluorescence concentration n of the tracer instead of molecular flux J and molecular concentration c. Due to the two-dimensional nature of the experiments, the interface length L_i has to be used instead of the interface area A, and similarly, concentration is given per area and not volume. Since we do not measure flux and concentration at the end of the plasmodesmata, but instead integrate all values for cell-to-cell diffusion over a certain interface, we can eliminate the diffusion distance Δx.

The tracer flux Q per micrometer is then given by

$$\frac{Q\ \tau^B}{L_i} = \mathrm{CFF}\ \Delta n \tag{3}$$

with the CCF in μm s^{-1} taking the place of the diffusion coefficient. The CCF comprises the molecule-specific diffusion constant plus other factors that influence the molecular flux driven by the concentration potential. In the case of cell coupling, the abundance of plasmodesmata and their transport capacity are the factors that primarily determine the permeability of a specific interface.

The factor τ^B corrects for the loss of tracer in the image plane of the neighbor cell (B) during photoactivation, due to diffusion into the next neighbors or uptake into the vacuole. It was determined for each cell type by measuring the signal loss in the cell during a postphotoactivation interval similar in length to the activation interval.

The cytosolic area of cells in the image plane, essential for the calculation of the cytosolic fluorescence concentration n, was determined as cell type-specific average with the help of the image-analysis software.

The course of photoactivation experiments is similar to fluorescence loss in photobleaching experiments that have been used to determine cell coupling before (Iliev and Wouters, 2007; Rutschow et al., 2011). In fluorescence loss in photobleaching experiments, no data can be acquired from the target cell during the bleaching phase because of signal saturation caused by the high laser intensity necessary for bleaching. Similarly, the target cell data during photoactivation cannot be used because of additional fluorescein excitation by the UV laser, but since tracer concentration in the target cell increases logarithmically (Fig. 1E; Liesche and Schulz, 2011), values can be extrapolated between the last preactivation frame and the first postactivation frame (dotted line in Fig. 1E). For the calculation of CCF after background subtraction, we find

$$\mathrm{CFF} = \frac{N_2^B \tau^B}{L_i} \frac{1}{(\bar{n}^A - \bar{n}^B)} \tag{4}$$

with N_2^B indicating the total signal intensity in the neighbor cell in the first frame after photoactivation and $\bar{n}^A$ and $\bar{n}^B$ indicating the average concentrations in the target cell (A) and neighbor cell (B), respectively.

Leaf Sap Osmolality

In the same way as described by Fu et al. (2011), samples were taken at mid afternoon, frozen in syringes, and thawed, and the leaf sap was pressed out. Osmolality was measured with a Gonotec Osmomat 030 cryoscopic osmometer.

Supplemental Data

The following materials are available in the online version of this article.

Supplemental Figure S1. Minor vein phloem of a minor vein from *V. faba* after photoactivation.

Supplemental Figure S2. Analysis of a photoactivation experiment in minor vein phloem of *C. maxima*.

Supplemental Movie S1. Movie showing photoactivation of a bundle-sheath cell of *C. maxima* (corresponding to Supplemental Figure S2).

ACKNOWLEDGMENTS

Kåre Hartvig Jensen from the Danish Technical University gave advice on the calculation of the CCF. We also thank Helle Juel Martens (University of Copenhagen) for critical reading of the manuscript. Imaging was performed at the Center for Advanced Bioimaging Denmark, University of Copenhagen.

Received February 5, 2012; accepted March 9, 2012; published March 15, 2012.

LITERATURE CITED

Ainsworth EA, Bush DR (2011) Carbohydrate export from the leaf: a highly regulated process and target to enhance photosynthesis and productivity. Plant Physiol **155:** 64–69

Ayre BG (2011) Membrane-transport systems for sucrose in relation to whole-plant carbon partitioning. Mol Plant **4:** 377–394

Bhatnagar SP, Moitra A (1996) Gymnosperms. New Age International, New Delhi

Blechschmidt-Schneider S, Eschrich W, Jahnke S (1997) Phloem loading, translocation and unloading processes. *In* H Rennenberg, W Eschrich, H Ziegler, eds, Trees: Contributions to Modern Tree Physiology. Backhuys Publishers, Leiden, The Netherlands, pp 139–163

Botha CEJ, van Bel AJ (1992) Quantification of symplastic continuity as visualised by plasmodesmograms: diagnostic value for phloem-loading pathways. Planta **187:** 359–366

Braun DM (2012) SWEET! The pathway is complete. Science **335:** 173–174

Canny MJ (1993) Transfusion tissue of pine needles as a site of retrieval of solutes from the transpiration stream. New Phytol **123:** 227–232

Chen LQ, Qu XQ, Hou BH, Sosso D, Osorio S, Fernie AR, Frommer WB (2012) Sucrose efflux mediated by SWEET proteins as a key step for phloem transport. Science **335:** 207–211

Davidson A, Keller F, Turgeon R (2011) Phloem loading, plant growth form, and climate. Protoplasma **248:** 153–163

Decourteix M, Alves G, Brunel N, Améglio T, Guillio A, Lemoine R, Pétel G, Sakr S (2006) JrSUT1, a putative xylem sucrose transporter, could mediate sucrose influx into xylem parenchyma cells and be up-regulated by freeze-thaw cycles over the autumn-winter period in walnut tree (*Juglans regia* L.). Plant Cell Environ **29:** 36–47

Delrot S, Bonnemain JL (1981) Involvement of protons as a substrate for the sucrose carrier during phloem loading in *Vicia faba* leaves. Plant Physiol **67:** 560–564

Dinant S, Lemoine R (2010) The phloem pathway: new issues and old debates. C R Biol **333:** 307–319

Ding B, Haudenshield JS, Hull RJ, Wolf S, Beachy RN, Lucas WJ (1992) Secondary plasmodesmata are specific sites of localization of the tobacco mosaic virus movement protein in transgenic tobacco plants. Plant Cell **4:** 915–928

Duckett CM, Oparka KJ, Prior DAM, Dolan L, Roberts K (1994) Dye-coupling in the root epidermis of Arabidopsis is progressively reduced during development. Development **120:** 3247–3255

Fu QS, Cheng LL, Guo YD, Turgeon R (2011) Phloem loading strategies and water relations in trees and herbaceous plants. Plant Physiol **157:** 1518–1527

Furch ACU, Hafke JB, Schulz A, van Bel AJE (2007) Ca^{2+}-mediated remote control of reversible sieve tube occlusion in *Vicia faba*. J Exp Bot **58:** 2827–2838

Gamalei Y (1989) Structure and function of leaf minor veins in trees and herbs: a taxonomic review. Trees Struct Funct **3:** 96–110

Geiger DR, Giaquinta RT, Sovonick SA, Fellows RJ (1973) Solute distribution in sugar beet leaves in relation to phloem loading and translocation. Plant Physiol **52:** 585–589

Giaquinta RT (1979) Phloem loading of sucrose: involvement of membrane ATPase and proton transport. Plant Physiol **63:** 744–748

Goodwin PB, Shepherd V, Erwee MG (1990) Compartmentation of fluorescent tracers injected into the epidermal cells of *Egeria densa* leaves. Planta **181:** 129–136

Haritatos E, Keller F, Turgeon R (1996) Raffinose oligosaccharide concentrations measured in individual cell and tissue types in *Cucumis melo* L. leaves: implications for phloem loading. Planta **198:** 614–622

Iliev AI, Wouters FS (2007) Application of simple photobleaching microscopy techniques for the determination of the balance between anterograde and retrograde axonal transport. J Neurosci Methods **161:** 39–46

Jackson RB, Schlesinger WH (2004) Curbing the U.S. carbon deficit. Proc Natl Acad Sci USA **101:** 15827–15829

Kim I, Kobayashi K, Cho E, Zambryski PC (2005) Subdomains for transport via plasmodesmata corresponding to the apical-basal axis are established during Arabidopsis embryogenesis. Proc Natl Acad Sci USA **102:** 11945–11950

Lederer B (1955) Vergleichende untersuchungen über das transfusionsgewebe einiger rezenter gymnospermen. *In* B Huber, ed, Vergleichend-Anatomische Untersuchungen. Gustav Fischer Verlag, Jena, Germany, pp 1–42

Liesche J, Martens HJ, Schulz A (2011) Symplasmic transport and phloem loading in gymnosperm leaves. Protoplasma **248:** 181–190

Liesche J, Schulz A (December 15, 2011) Quantification of plant cell coupling with three-dimensional photoactivation microscopy. J Microsc http://dx.doi.org/10.1111/j.1365-2818.2011.03584.x

Martens HJ, Hansen M, Schulz A (2004) Caged probes: a novel tool in studying symplasmic transport in plant tissues. Protoplasma **223:** 63–66

Martens HJ, Roberts AG, Oparka KJ, Schulz A (2006) Quantification of plasmodesmatal endoplasmic reticulum coupling between sieve elements and companion cells using fluorescence redistribution after photobleaching. Plant Physiol **142:** 471–480

Münch E (1930) Die Stoffbewegungen in der Pflanze. Gustav Fischer, Jena, Germany

Okumoto S (2010) Imaging approach for monitoring cellular metabolites and ions using genetically encoded biosensors. Curr Opin Biotechnol **21:** 45–54

Oparka KJ, Prior DA (1992) Direct evidence for pressure-generated closure of plasmodesmata. Plant J **2:** 741–750

Oparka KJ, Turgeon R (1999) Sieve elements and companion cells: traffic control centers of the phloem. Plant Cell **11:** 739–750

Orlich G, Hofbrückl M, Schulz A (1998) A symplasmic flow of sucrose contributes to phloem loading in Ricinus. Planta **206:** 108–118

Pawley JB (2006) Handbook of Biological Confocal Microscopy, Ed 3. Springer, New York

Payyavula RS, Tay KHC, Tsai CJ, Harding SA (2011) The sucrose transporter family in Populus: the importance of a tonoplast PtaSUT4 to biomass and carbon partitioning. Plant J **65:** 757–770

Pina A, Errea P, Schulz A, Martens HJ (2009) Cell-to-cell transport through plasmodesmata in tree callus cultures. Tree Physiol **29:** 809–818

Rennie EA, Turgeon R (2009) A comprehensive picture of phloem loading strategies. Proc Natl Acad Sci USA **106:** 14162–14167

Rinne PL, van der Schoot C (1998) Symplasmic fields in the tunica of the shoot apical meristem coordinate morphogenetic events. Development **125:** 1477–1485

Roberts AG, Oparka KJ (2003) Plasmodesmata and the control of symplastic transport. Plant Cell Environ **26:** 103–124

Rutschow HL, Baskin TI, Kramer EM (2011) Regulation of solute flux through plasmodesmata in the root meristem. Plant Physiol **155:** 1817–1826

Schneider A, Schmitz K (1989) Seasonal course of translocation and distribution of C-14-labelled photoassimilate in young trees of *Larix decidua* Mill. Trees Struct Funct **3:** 185–191

Schulz A (1990) Conifers. *In* H-D Behnke, RD Sjolund, eds, The Sieve Element: Comparative Structure, Induction and Development. Springer Verlag, Berlin, pp 63–88

Schulz A (1994) Phloem transport and differential unloading in pea-seedlings after source and sink manipulations. Planta **192:** 239–248

Schulz A (1995) Plasmodesmal widening accompanies the short-term increase in symplasmic phloem unloading in pea root-tips under osmotic stress. Protoplasma **188:** 22–37

Schulz A (1999) Physiological control of plasmodesmal gating. *In* AJE van Bel, WJP Van Kesteren, eds, Plasmodesmata: Structure, Function, Role in Cell Communication. Springer, Berlin, pp 173–204

Schulz A (2005) Role of plasmodesmata in solute loading and unloading. *In* K Oparka, ed, Plasmodesmata. Blackwell Publishing, Oxford, pp 135–161

Schulz A, Kuhn C, Riesmeier JW, Frommer WR (1998) Ultrastructural effects in potato leaves due to antisense-inhibition of the sucrose transporter indicate an apoplasmic mode of phloem loading. Planta **206:** 533–543

Schumacher W (1950) Zur Bewegung des Fluroesceins in den Siebröhren. Planta **37:** 626–634

Shaukat SS, Moore KG, Lovell PH (1975) Some effects of triazines on growth, photosynthesis and translocation of photosynthate in Pinus species. Physiol Plant **33:** 295–299

Shiroya T, Lister GR, Slankis V, Krotkov G, Nelson CD (1962) Translocation of the products of photosynthesis to roots of pine seedlings. Can J Bot **40:** 1125–1135

Terry BR, Robards AW (1987) Hydrodynamic radius alone governs the mobility of molecules through plasmodesmata. Planta **171:** 145–157

Testa I, Parazzoli D, Barozzi S, Garrè M, Faretta M, Diaspro A (2008) Spatial control of pa-GFP photoactivation in living cells. J Microsc **230:** 48–60

Tucker JE, Mauzerall D, Tucker EB (1989) Symplastic transport of carboxyfluorescein in staminal hairs of *Setcreasea purpurea* is diffusive and includes loss to the vacuole. Plant Physiol **90:** 1143–1147

Turgeon R (2010) The role of phloem loading reconsidered. Plant Physiol **152:** 1817–1823

Turgeon R, Beebe DU (1991) The evidence for symplastic phloem loading. Plant Physiol **96:** 349–354

Turgeon R, Beebe DU, Gowan E (1993) The intermediary cell: minor-vein anatomy and raffinose oligosaccharide synthesis in the Scrophulariaceae. Planta **191:** 446–456

Turgeon R, Hepler PK (1989) Symplastic continuity between mesophyll and companion cells in minor veins of mature *Cucurbita pepo* L. leaves. Planta **179:** 24–31

Turgeon R, Medville R (1998) The absence of phloem loading in willow leaves. Proc Natl Acad Sci USA **95:** 12055–12060

Turgeon R, Medville R (2004) Phloem loading: a reevaluation of the relationship between plasmodesmatal frequencies and loading strategies. Plant Physiol **136:** 3795–3803

Turgeon R, Wolf S (2009) Phloem transport: cellular pathways and molecular trafficking. Annu Rev Plant Biol **60:** 207–221

van Bel AJE (1993) Strategies of phloem loading. Annu Rev Plant Physiol Plant Mol Biol **44:** 253–281

Voitsekhovskaja OV, Koroleva OA, Batashev DR, Knop C, Tomos AD, Gamalei YV, Heldt HW, Lohaus G (2006) Phloem loading in two Scrophulariaceae species: what can drive symplastic flow via plasmodesmata? Plant Physiol **140:** 383–395

Willenbrink J (2002) Assimilate transport in phloem: regulation and mechanism. Russ J Plant Physiol **49:** 8–15

Wu XQ, Lin J, Lin Q, Wang J, Schreiber L (2005) Casparian strips in needles are more solute permeable than endodermal transport barriers in roots of *Pinus bungeana*. Plant Cell Physiol **46:** 1799–1808